Extended wavelength mid-infrared photoluminescence from Type-I InAsN and InGaAsN dilute nitride quantum wells grown on InP

R. Wheatley[1], M. Kesaria[1*], L. J. Mawst[2], J. D. Kirch[2], T. F.Kuech[3], A. Marshall[1], Q. D. Zhuang[1] and A. Krier[1],

[1]*Physics Department, Lancaster University, Lancaster, LA1 4YB, U. K.*

[2]*Department of Electrical and Computer Engineering, 1415 Engineering Drive, Madison, University of Wisconsin, WI 53706, Wisconsin, U. S. A.*

[3]*Department of Chemical and Biological Engineering, 1415 Engineering Drive, Madison, University of Wisconsin, WI 53706, Wisconsin, U. S. A.*

*Corresponding author: *m.kesaria@lancaster.ac.uk*

Extended wavelength photoluminescence emission within the technologically important 2-5 μm spectral range has been demonstrated from $InAs_{1-x}N_x$ and $In_{1-y}Ga_yAs_{1-x}N_x$ type I quantum wells grown onto InP. Samples containing N~1 % and 2 % exhibited 4 K photoluminescence emission at 2.0 and 2.7 μm, respectively. The emission wavelength was extended out to 2.9 μm (3.3 μm at 300 K) using a metamorphic buffer layer to accommodate the lattice mismatch. The quantum wells were grown by molecular beam epitaxy and found to be of a high structural perfection as evidenced in the high resolution x-ray diffraction measurements. The photoluminescence was more intense from the quantum wells grown on the metamorphic buffer layer and persisted up to room temperature. The mid-infrared emission spectra were analysed and the observed transitions were found to be in good agreement with the calculated emission energies.

There is increasing interest in compact semiconductor light sources operating within the 2–5 μm wavelength range due to their potential for applications in chemical gas analysis, medical diagnostics and pollution monitoring. Lasers [1,2] and LEDs [3-6] have been developed using device architectures with different levels of complexity [7-9] on InAs or GaSb substrates for which the processing technology is relatively immature [10-12]. By comparison, InP based technology is well developed for optical communication systems at 1.33–1.55 μm and consequently there has been much effort dedicated towards extending the wavelength of InP based light sources out beyond 2 μm using InGaAs/InAlAs type I and InGaAs/GaAsSb, GaInAs/GaAsSb type II quantum well (QW) structures [4]. Access to longer wavelengths using type I QWs is often limited by Auger recombination or shallow band offsets and in type II systems by a reduced electron-hole wavefunction overlap. Quantum Cascade Lasers (QCLs)

on an InP substrate show high performance in the 4-5 μm wavelength region [13], but become quite challenging for wavelengths shorter than 3.5 μm due to high lattice-mismatch strain [14-16]. Therefore, it is important to explore alternative material systems, such as the dilute nitrides, to alleviate these problems and extend the available wavelength range. The incorporation of nitrogen into III-V semiconductors results in a reduction of the bandgap due to band anti-crossing effects associated with the interaction between the conduction band of the host and localized states introduced by the nitrogen [17]. This approach has been the subject of a number of investigations resulting in reports of InP-based mid-infrared light emission using InAsN, InAsSbN, GaInAsN and InGaAsNSb quantum wells [18-25,26]. It is highly desirable to maintain type I recombination because of the high oscillator strength. The maximum wavelength achieved to date in such InAsN and InGaAsN systems on InP is ~2.6 μm at 260 K [20,21,24,27,28]. This maximum wavelength is limited due to the critical layer thickness and material quality of such highly-strained structures. The defect density within dilute nitride materials increases with N concentration increasing beyond 2 %.

In this study, we report on type I QW structures using In-rich $In_yGa_{1-y}As_{1-x}N_x$ / $In_yGa_{1-y}As$ MQW containing N~1 % and 2 % grown on InP substrates and demonstrate 4 K photoluminescence emission at 2.0 and 2.7 μm, respectively. We also show that the emission wavelength can be extended to 2.9 μm (3.3 μm at 300 K) using an $InAs_{1-x}N_x$ / $In_yGa_{1-y}As$ MQW (with N~1 %) structure grown on a reduced-dislocation-density metamorphic buffer layer (MBL). The optical and structural properties were investigated using low temperature photoluminescence (PL) and high resolution x-ray diffraction (HRXRD).

A VG-V80H solid-source molecular-beam-epitaxy (MBE) reactor equipped with a Veeco UNI-bulb radio-frequency (RF) plasma nitrogen-source was used to grow the N-containing quantum well structures on InP substrates as shown in Figure 1. The epitaxial growth was based on our previous work, where we reported on MBE-grown $InAs_{1-x}N_x$ bulk layers with N-content from 0.2 % to 1 % on semi-insulating (100) GaAs [29]. The $In_yGa_{1-y}As_{1-x}N_x$ growth was carried out at a substrate temperature of 420 ℃, using a growth rate of 0.5 μmh^{-1} and minimum As flux with a fixed nitrogen plasma setting (forward power of 160 W and a nitrogen flux of 5.0×10^{-7} mbar). Nitrogen incorporation was controlled by adjusting the growth rates and plasma settings under an optimized set of growth conditions. The growth of $In_yGa_{1-y}As_{1-x}N_x$ MQW dilute nitride layers was performed using similar conditions to those used for $InAs_{1-x}N_x$ layers [30,31], where the lattice matched $In_{0.53}Ga_{0.47}As$ was calibrated prior to growth of all three samples. A schematic diagram showing the design of each of the MQW structures is shown in Figure 1. Sample (a) has a 1μm undoped lattice matched $In_{0.53}Ga_{0.47}As$ buffer layer grown at 480 ℃ before the substrate temperature was reduced to 420 ℃ to commence growth of ten-period MQWs with 25nm $In_{0.53}Ga_{0.47}As$ barriers and 7nm $In_{0.70}Ga_{0.30}As_{0.99}N_{0.01}$ quantum wells, capped with 100nm $In_{0.53}Ga_{0.47}As$. The structure of sample (b) is similar to (a) with the exception of the quantum well composition which was $In_{0.80}Ga_{0.20}As_{0.98}N_{0.02}$. Sample (c) was grown at 480 ℃ on top of an MOVPE-grown metamorphic buffer layer (MBL), starting with a 10 nm undoped $In_{0.77}Ga_{0.23}As$ layer followed by ten QWs with 20nm $In_{0.77}Ga_{0.23}As$ barriers and 10 nm $InAs_{0.99}N_{0.01}$ wells capped with 20nm $In_{0.77}Ga_{0.23}As$. The MBL consists of 10-step compositionally-graded $InP_{1-y}Sb_y$ (y

= 0.0 to 0.2) terminating with an $InAs_{0.5}P_{0.5}$ (500 nm) capping layer. The MOVPE growth, structural and optical properties as well as details of the design of the MBL on InP substrate have been reported previously elsewhere [32]. The nitrogen composition, lattice mismatch and strain in the resulting MQWs were examined using high resolution x-ray diffraction (HRXRD). Photoluminescence (PL) spectroscopy measurements were made using an Ar^+ ion laser at an excitation wavelength λ=514 nm and maximum power density P=20 W cm^{-2} at the sample surface. The PL emission was analysed using a 0.3 m Bentham M300 monochromator and detected by a cooled (77 K) InSb photodiode coupled with a Stanford Research (SR850) digital lock-in amplifier. Samples were cooled in a variable temperature (4 ─ 300 K) continuous flow He cryostat.
The X-ray diffraction (ω ─ 2Θ scans) of samples (a) and (b) are shown in Figure 2. (The XRD spectrum from sample (c) was similar to that of sample (a) and is not shown here). Both patterns are referenced at 0 arc sec for the (004) reflection from the InP substrate. They exhibit an intense and equal number of satellite peaks, characteristic of abrupt interfaces and low defect density. The full width at half maximum (FWHM) of the distinct satellite peaks is 55 arc sec. The nitrogen, gallium and indium composition in these samples was determined by fitting, using Bede RADS simulation software which is based on dynamical scattering theory of X-ray diffraction. The corresponding simulated spectra are shown in blue along with the experimentally acquired XRD pattern (black). The resulting N, In and Ga composition in each sample is as shown in Figure 1.

Figure 3, shows the normalised 4 K PL spectra from each of the samples. The PL intensity of sample (c) grown on the MBL is 6 times higher than (a) and 21 times higher than (b) which were grown directly on the InP substrate. The PL linewidth of the MBL sample (c) is the narrowest amongst all three samples, which indicates that it has the lowest defect density and other forms of disorder attributable, in part, to both the growth process and the MBL design as reported by Kirch et al [32,33]. The PL peak energy of sample (b) containing 2 % N is lower than that of sample (a) with 1 % N, consistent with the N-induced band anti-crossing models. The incorporation of N in $In_{1-y}Ga_yAs$ also introduces local strain due to the large difference in atomic radius between N (65 pm) and As (133 pm), which results in a higher defect density within the grown layer. Consequently, the PL intensity is lower and the linewidth in (b) is larger than in sample (a) due to the higher compositional disorder from the increased N content.

The PL transition energies were calculated using a Schrodinger solver within the effective mass approximation, starting with m^*_e=0.029 m_o for bulk InAsN layers containing N=1 % [34] and taking account of band anti-crossing effects and strain[12, 35-39]. The results are illustrated in Figure 4 and the corresponding transition energies are given in Table I. The observed PL peak energies are in approximate agreement with the e1-hh1 transitions in each case. The difference in calculated and experimental values can be accounted for by uncertainties in the N content and accurate knowledge of the effective masses within the QW and barriers.

Table I: Properties of the samples and parameters estimated from PL measurement.

Sample	N content in QW ± 0.1%	Calculated PL transition energy (eV) at 4 K	4 K PL Peak Energy (eV) (expt.) ± 0.01	4 K PL Line width (meV)	Activation energy (meV)	QW strain (%)	PL Peak Intensity (4 K) ± 0.01
a	1.0%	0.632	0.622	24.0	9.0	1.0	10.8
b	2.0%	0.489	0.468	27.0	8.0	1.4	2.9
c	1.0% on MBL	0.430	0.423	13.0	42.0	1.2	60.5

The dependence of the PL emission intensity using different laser excitation power from 0.2 W to 1.8 W was investigated. None of the samples exhibited a measurable change in peak position (2.05 μm, 2.68 μm and 2.93 μm for a, b and c, respectively). This is unlike the case of bulk $InAs_{1-x}N_x$ layers, where the activation of localised states is apparent in a peak shift attributed to an increased carrier concentration [39]. Previous reports have however indicated that the PL peak energy can remain unchanged with variation in excitation power for $InAs_{1-x}N_x$ / $In_{1-y}Ga_yAs$ MQWs on InP substrate [27]. In power dependent PL measurements, the input pump power (I) and luminescence intensity (L) can be related by $I \sim L^k$, where sub-linear k parameters ($k < 1$) are characteristic of free-to-bound or donor-to-acceptor recombination. Free exciton recombination exhibits a $k \geq 1$ [40]. Analysis of Fig. 5 shows that $k = 1$ consistent with free exciton recombination at low temperature for all samples [40].

The temperature dependence of the integrated PL intensity for each of the samples is shown in Figure 6. Room temperature PL was not observable for samples (a) and (b) and the emission became thermally quenched above 120 K. However, the PL of MBL sample (c) was more intense and PL emission was readily observed at room temperature. The quantitative estimate of the activation energies (E_a) was obtained from Arrhenius plots of the *ln* of the PL intensity versus the reciprocal absolute temperature. The activation energy values are given in Table I. The thermal quenching of samples (a) and (b) were similar and since all samples have approximately the same e-h confinement, as shown in Figure 4. We attribute the small activation energy of 8−9 meV in these cases to non-radiative SRH recombination within the barriers. For sample (c) grown on the MBL buffer, the thermal quenching was reduced and the PL easily persisted up to room temperature. In this case, the PL quenching was attributed to loss of hole confinement within the valence band potential well which is consistent with the calculated hole confinement and valence band offsets (see Table 1 and Figure 4).

We have demonstrated the MBE growth of In(Ga)AsN MQWs on InP for N contents up to 2 % using both direct growth on an InP substrate or on a MOVPE-grown metamorphic buffer layer. Although the high resolution X-ray diffraction patterns obtained from samples obtained using direct growth exhibit very good diffraction pattern and PL at 4 K, the emission from these samples did not persist to room temperature. The rather low activation energy of 8-9

meV for thermal quenching of the PL is not consistent with loss of electrons/holes from the QW and is attributed to non-radiative recombination in the barriers. By comparison, the sample grown on the MOVPE MBL buffer exhibited more intense PL at 4 K and with a substantially narrower linewidth consistent with reduced non-radiative recombination and higher structural perfection of the MQWs. The quenching of the PL in these samples is related to loss of hole confinement (~2 k_B.T) near room temperature. The observed optical transitions were found to be in good agreement with the calculated emission energies and demonstrate that the accessible spectral range can be extended into the mid–infrared using InP substrates whose performance is enhanced when employing a metamorphic buffer layer.

Acknowledgement

We are grateful to the UK Engineering and Physical Sciences Research Council (EPSRC) for financial support (grant EP/J015849/1).

References:

[1] G. R. Nash, S. J. B. Przeslak, S. J. Smith, G. de Valicourt, A. D. Andreev, P. J. Carrington, M. Yin, A. Krier, S. D. Coomber, L. Buckle, M. T. Emeny, and T. Ashley, Applied Physics Letters **94,** 091111 (2009).

[2] L. J. Mawst, Photonics Journal, IEEE **2,** 213 (2010).

[3] H. Takasaki, Y. Kawamura, T. Katayama, A. Yamamoto, and N. Inoue, Journal of Crystal Growth **227–228,** 294 (2001).

[4] C. Grasse, P. Wiecha, T. Gruendl, S. Sprengel, R. Meyer, and M.-C. Amann, Applied Physics Letters **101**, 221107 (2012).

[5] Q. Lu, Q. Zhuang, J. Hayton, M. Yin, and A. Krier, Applied Physics Letters **105,** 031115 (2014).

[6] Q. Lu, Q. Zhuang, A. Marshall, M. Kesaria, R. Beanland, and A. Krier, Semiconductor Science And Technology **29,** 075011 (2014).

[7] D. Paul, in *Physics and Applications of Terahertz Radiation*; *Vol. 173*, edited by M. Perenzoni and D. J. Paul (Springer Netherlands, 2014), p. 103.

[8] J. Abell, C. S. Kim, W. W. Bewley, C. D. Merritt, C. L. Canedy, I. Vurgaftman, J. R. Meyer, and M. Kim, Applied Physics Letters **104,** 261103 (2014).

[9] I. Vurgaftman, R. Weih, M. Kamp, J. R. Meyer, C. L. Canedy, C. S. Kim, M. Kim, W. W. Bewley, C. D. Merritt, J. Abell, and S. Höfling, Journal of Physics D: Applied Physics **48,** 123001 (2015).

[10] L. Naehle, S. Belahsene, M. v. Edlinger, M. Fischer, G. Boissier, P. Grech, G. Narcy, A. Vicet, Y. Rouillard, J. Koeth, and L. Worschech, in *Electronics Letters*; *Vol. 47* (Institution of Engineering and Technology, 2011), p. 46.

[11] A. Krier, M. Yin, V. Smirnov, P. Batty, P. J. Carrington, V. Solovev, and V. Sherstnev, physica status solidi (a) **205,** 129 (2008).

[12] A. Krier, M. d. l. Mare, P. J. Carrington, M. Thompson, Q. Zhuang, A. Patanè, and R. Kudrawiec, Semiconductor Science And Technology **27,** 094009 (2012).

[13] A. Lyakh, R. Maulini, A. Tsekoun, R. Go, C. Pflügl, L. Diehl, Q. J. Wang, F. Capasso, and C. K. N. Patel, Applied Physics Letters **95,** 141113 (2009).

[14] A. Bismuto, M. Beck, and J. Faist, Applied Physics Letters **98,** 191104 (2011).

[15] N. Bandyopadhyay, S. Slivken, Y. Bai, and M. Razeghi, Applied Physics Letters **100,** 212104 (2012).
[16] N. Bandyopadhyay, Y. Bai, S. Tsao, S. Nida, S. Slivken, and M. Razeghi, Applied Physics Letters **101,** 241110 (2012).
[17] W. Shan, K. M. Yu, W. Walukiewicz, J. Wu, I. J. W. Ager, and E. E. Haller, Journal of Physics: Condensed Matter **16,** S3355 (2004).
[18] T. Shono, S. Mizuta, and Y. Kawamura, Journal of Crystal Growth **378,** 69 (2013).
[19] Y. Kawamura, Electronics and Communications in Japan **94,** 33 (2011).
[20] S. Ding-Kang, L. Hao-Hsiung, and Y. H. Lin, Electronics Letters **37,** 1342 (2001).
[21] G.R. Chen, H. H. Lin, J.S. Wang and D. K. Shih, Journal of Electronic Materials **32**, 244, (2003).
[22] K. Yuichi and I. Naohisa, Japanese Journal of Applied Physics **46,** 3380 (2007).
[23] J.S. Wang and H.H. Lin, Journal of Vacuum Science Technology B **17,** 1997 (1999).
[24] J.S. Wang, H.H. Lin, L.W. Song, and G.R. Chen, Journal of Vacuum Science Technology B **19,** 202 (2001).
[25] S. Z. Wang, S. F. Yoon, W. J. Fan, C. Y. Liu, and S. Yuan, Journal of Vacuum Science & Technology B **23,** 1434 (2005).
[26] K. Yuichi and S. Toru, Japanese Journal of Applied Physics **53,** 028004 (2014).
[27] D.K. Shih, H.H. Lin, and Y.H. Lin, *IEE Proceedings – Optoelectronics,**150***, 253, (2003).
[28] K. Köhler, J. Wagner, P. Ganser, D. Serries, T. Geppert, M. Maier, and L. Kirste, Journal of Physics: Condensed Matter **16,** S2995 (2004).
[29] M. de la Mare, Q. Zhuang, A. Krier, A. Patane, and S. Dhar, Applied Physics Letters **95,** 031110 (2009).
[30] M. d. l. Mare, Q. Zhuang, A. Patanè, and A. Krier, Journal of Physics D: Applied Physics **45,** 395103 (2012).
[31] A. Fleck, B. J. Robinson, and D. A. Thompson, Applied Physics Letters **78,** 1694 (2001).
[32] J. Kirch, T. W. Kim, J. Konen, L. J. Mawst, T. F. Kuech, and T. S. Kuan, Journal of Crystal Growth **315,** 96 (2011).
[33] J. Kirch, T. Garrod, S. Kim, J. H. Park, J. C. Shin, L. J. Mawst, T. F. Kuech, X. Song, S. E. Babcock, I. Vurgaftman, J. R. Meyer, and T.-S. Kuan, Journal of Crystal Growth **312,** 1165 (2010).
[34] A. Patanè, W. H. M. Feu, O. Makarovsky, O. Drachenko, L. Eaves, A. Krier, Q. D. Zhuang, M. Helm, M. Goiran, and G. Hill, Physical Review B **80,** 115207 (2009).
[35] M. P. C. M. Krijn, Semiconductor Science And Technology **6** (1), 27 (1991).
[36] I. Vurgaftman, J. R. Meyer, and L. R. Ram-Mohan, Journal of Applied Physics **89** (11), 5815 (2001).
[37] J. Ibáñez, R. Oliva, M. De la Mare, M. Schmidbauer, S. Hernández, P. Pellegrino, D. J. Scurr, R. Cuscó, L. Artús, M. Shafi, R. H. Mari, M. Henini, Q. Zhuang, A. Godenir, and A. Krier, Journal of Applied Physics **108** (10), 103504 (2010).
[38] W. Shan, W. Walukiewicz, J. W. Ager, E. E. Haller, J. F. Geisz, D. J. Friedman, J. M. Olson, and S. R. Kurtz, Physical Review Letters **82** (6), 1221 (1999).
[39] Q. Zhuang, A. Godenir, and A. Krier, Journal of Physics D: Applied Physics **41,** 132002 (2008).
[40] T. Schmidt, K. Lischka, and W. Zulehner, Physical Review B **45,** 8989 (1992).

Figures with captions

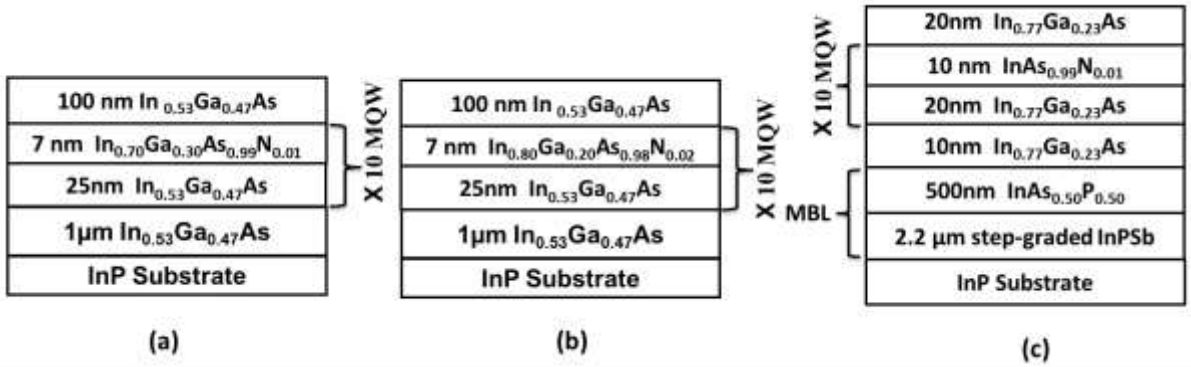

Fig. 1. A schematic of the different structures, each containing ten In(Ga)AsN QWs. Samples (a) and (b) contained 1% and 2% N in the QW respectively and were grown directly onto InP by MBE. Sample (c) contained 1% N in the QW which was grown by MBE on top of an MOVPE-grown metamorphic buffer [33].

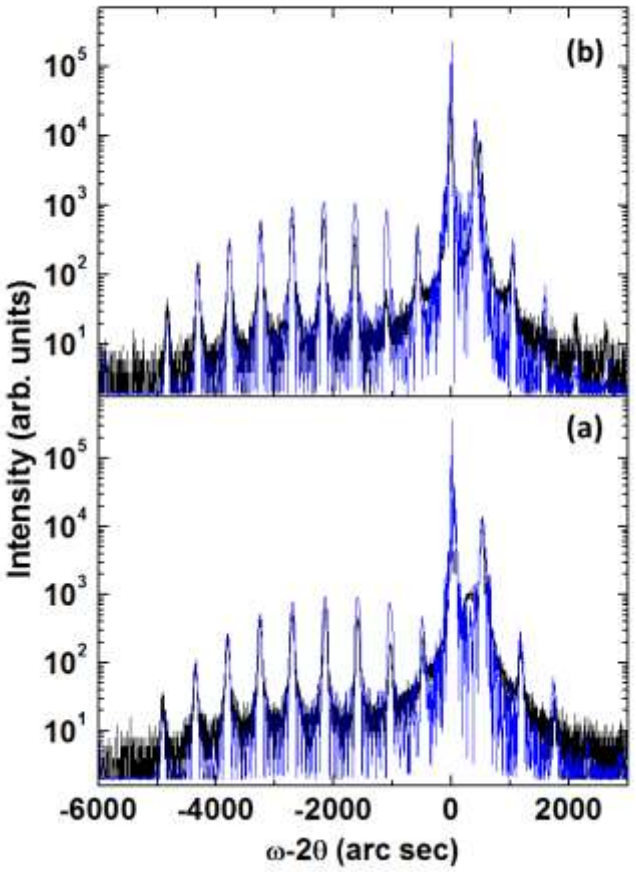

Fig. 2 HRXRD patterns of the InGaAsN/InGaAs MQW structures (a) 1 % N and (b) 2 % N shown in black along with corresponding simulations (blue).

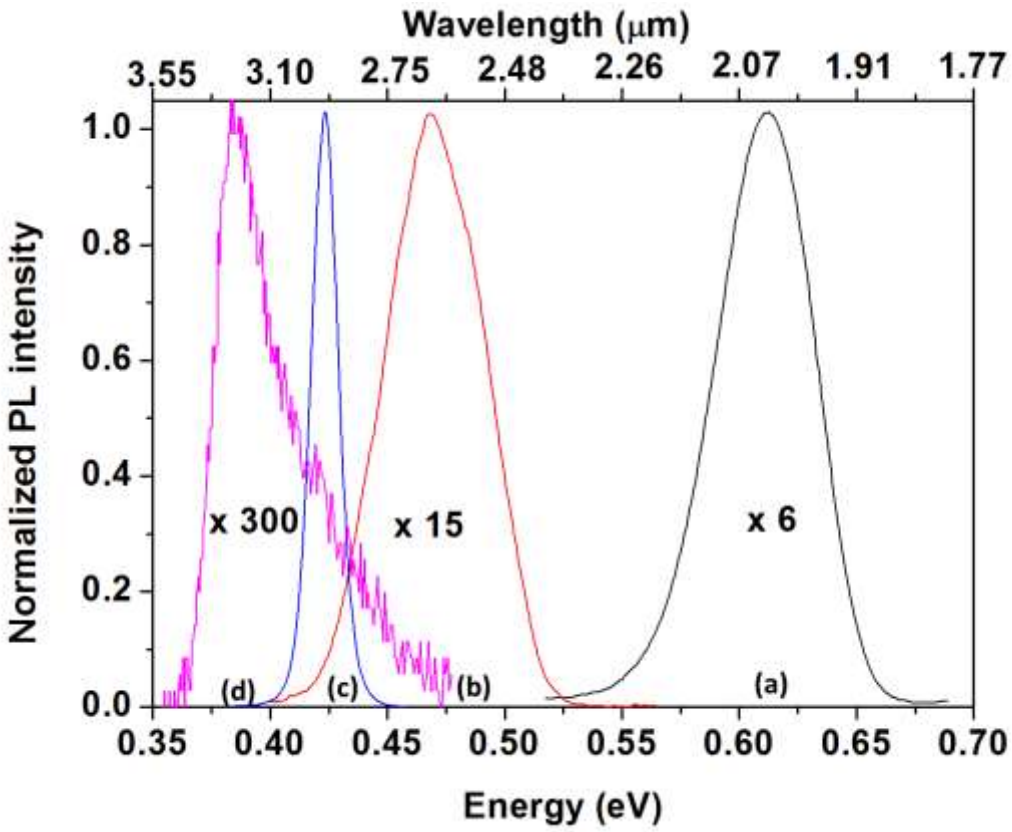

Fig. 3. The normalized 4K PL spectra from each of the samples (a) 1 % N (black), (b) 2 % N (red) and (c) 1 % N on MBL (blue). The peak energies and linewidths are given in Table 1 below. Spectrum (d) is the normalized 300 K PL spectrum of sample (c) and is shown pink.

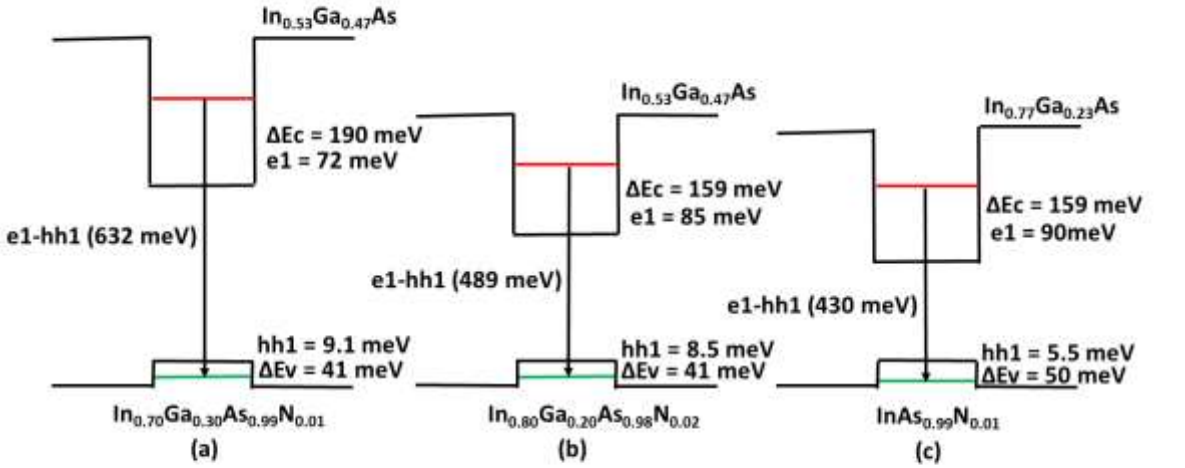

Fig. 4. A schematic diagram showing the calculated band structure and confinement energies for the lowest confined electron, (e1) and heavy hole, (hh1) states for each of the samples.

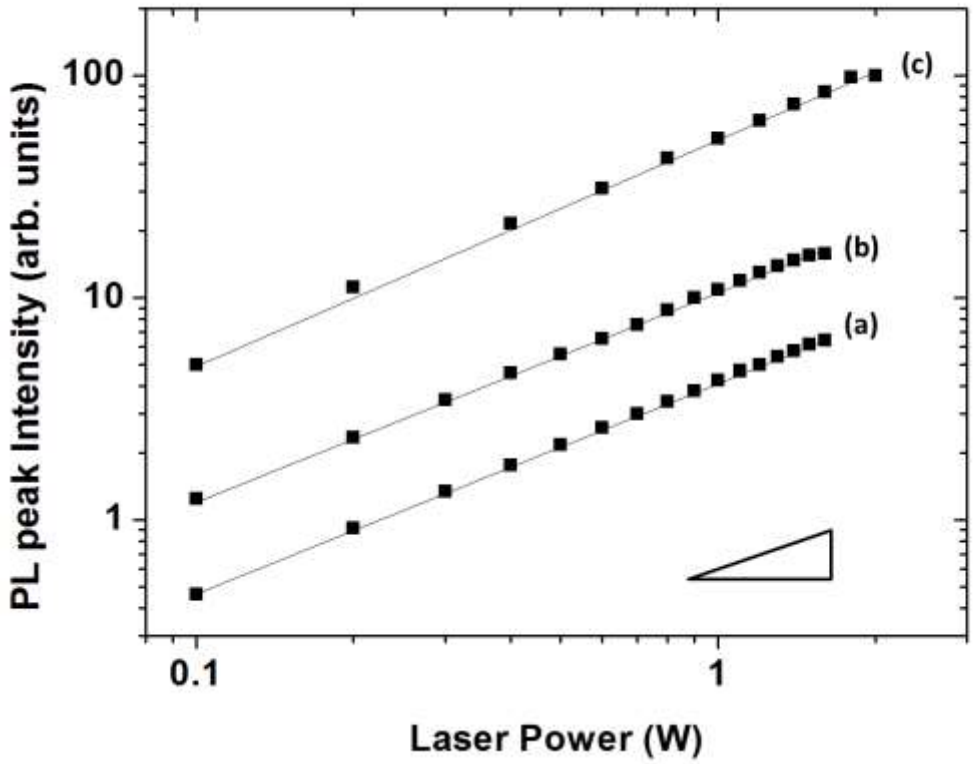

Fig. 5. The dependence of the 4 K PL peak emission intensity vs excitation power for each of the samples. In each case the slope, k=1. (a) 1%N, (b) 2%N and (c) 1%N on MBL. The triangle indicates a slope of k=1.

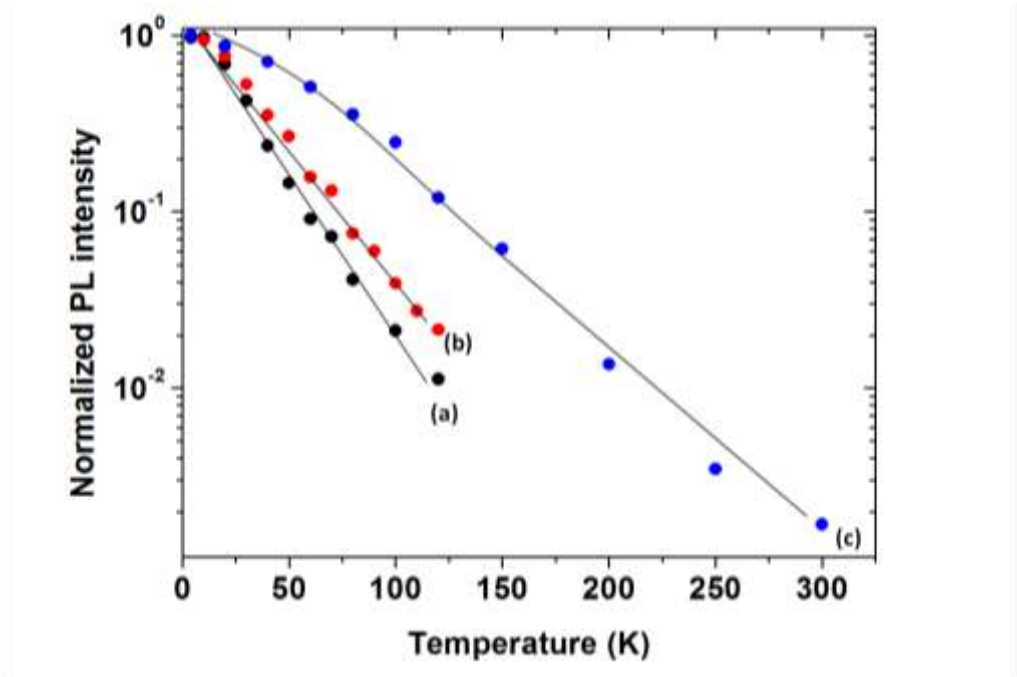

Fig. 6. The temperature dependence of the normalised integrated PL intensity for samples (a) 1 % N, (b) 2 % N and (c) 1 % N on MBL.

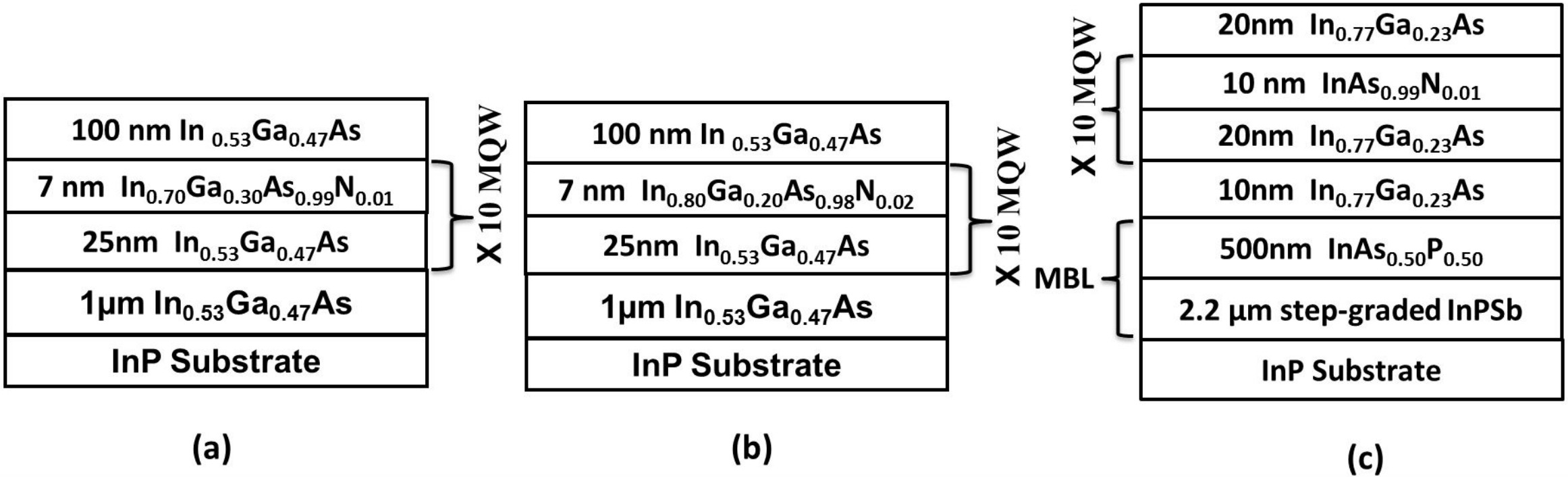
100 nm In 0.53Ga0.47As
7 nm In0.70Ga0.30As0.99N0.01
25nm In0.53Ga0.47As
X 10 MQW
1µm In0.53Ga0.47As
InP Substrate
(a)
100 nm In 0.53Ga0.47As
7 nm In0.80Ga0.20As0.98N0.02
25nm In0.53Ga0.47As
X 10 MQW
1µm In0.53Ga0.47As
InP Substrate
(b)
20nm In0.77Ga0.23As
10 nm InAs0.99N0.01
X 10 MQW
20nm In0.77Ga0.23As
10nm In0.77Ga0.23As
500nm InAs0.50P0.50
MBL
2.2 µm step-graded InPSb
InP Substrate
(c)

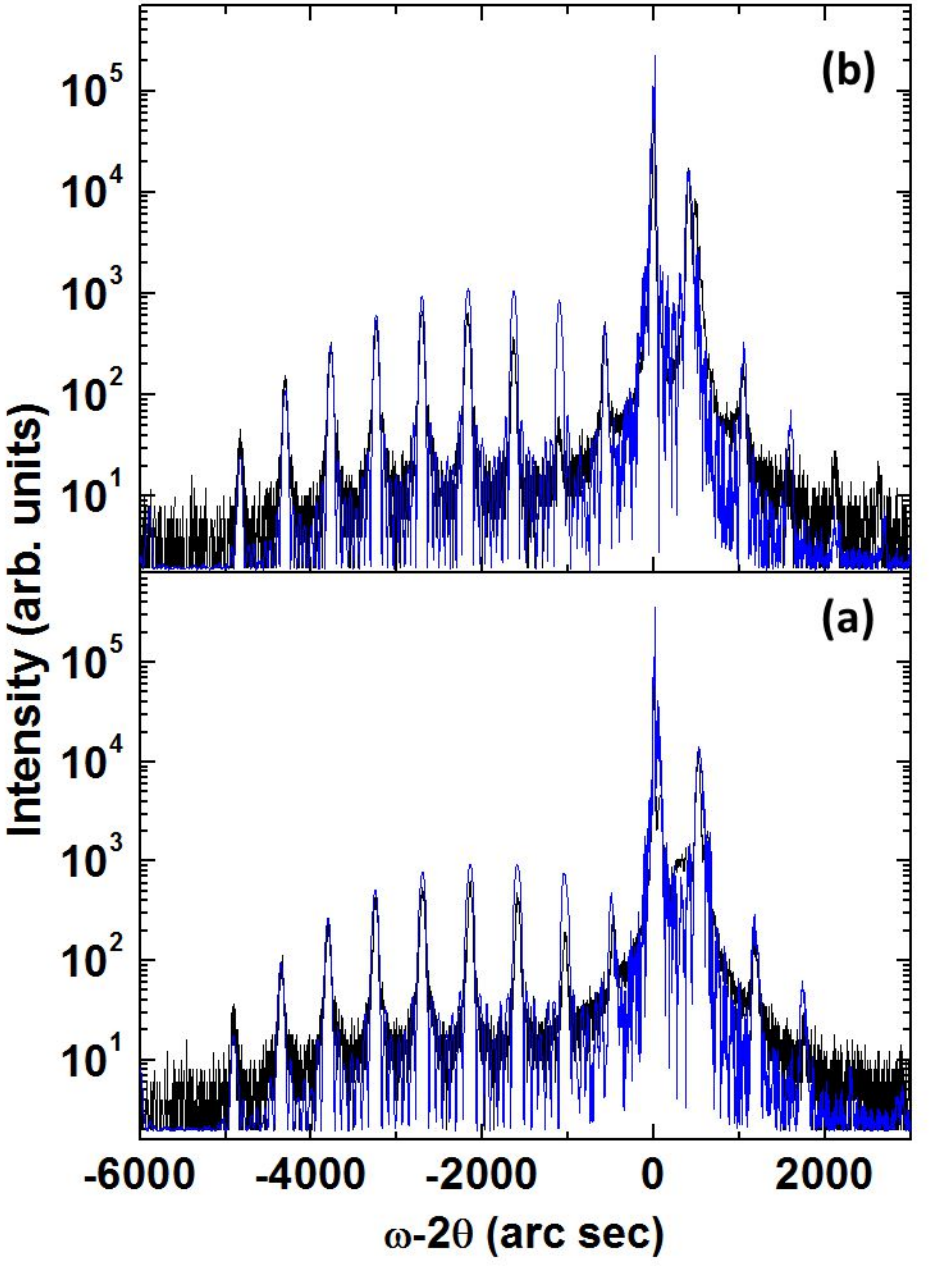
(b)
(a)
Intensity (arb. units)
10^5
10^4
10^3
10^2
10^1
-6000
-4000
-2000
0
2000
ω-2θ (arc sec)

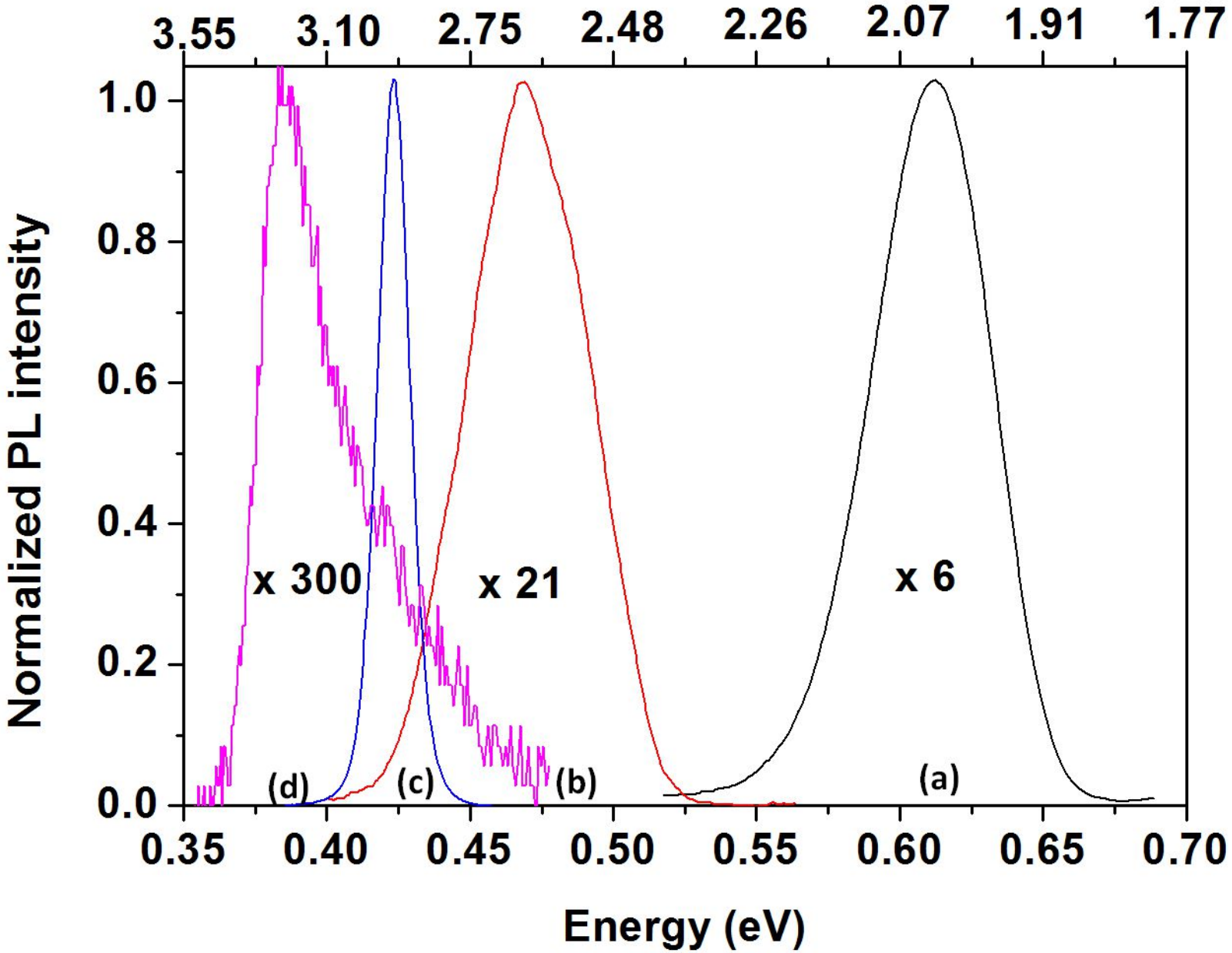
3.55
3.10
2.75
2.48
2.26
2.07
1.91
1.77
1.0
0.8
0.6
0.4
0.2
0.0
Normalized PL intensity
x 300
x 21
x 6
(d)
(c)
(b)
(a)
0.35
0.40
0.45
0.50
0.55
0.60
0.65
0.70
Energy (eV)

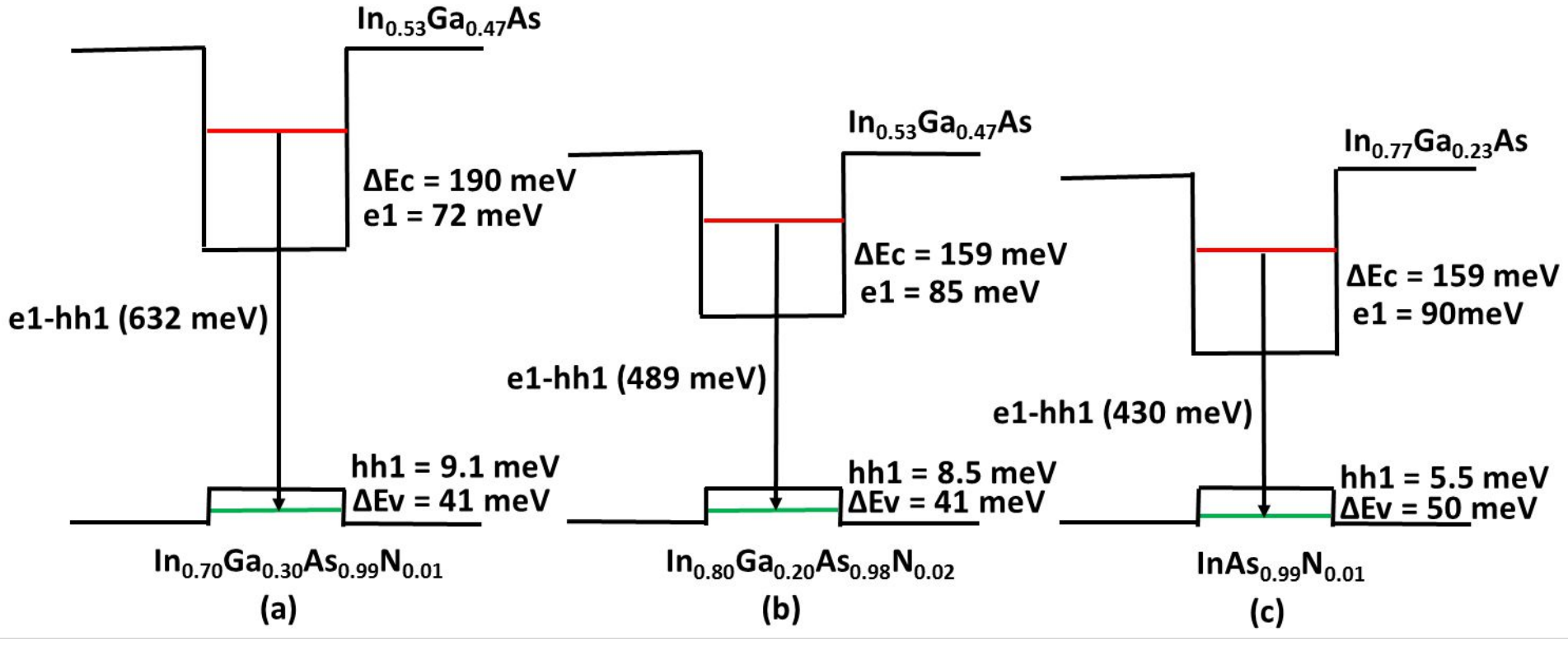
$In_{0.53}Ga_{0.47}As$
ΔEc = 190 meV
e1 = 72 meV
e1-hh1 (632 meV)
hh1 = 9.1 meV
ΔEv = 41 meV
$In_{0.70}Ga_{0.30}As_{0.99}N_{0.01}$
(a)
$In_{0.53}Ga_{0.47}As$
ΔEc = 159 meV
e1 = 85 meV
e1-hh1 (489 meV)
hh1 = 8.5 meV
ΔEv = 41 meV
$In_{0.80}Ga_{0.20}As_{0.98}N_{0.02}$
(b)
$In_{0.77}Ga_{0.23}As$
ΔEc = 159 meV
e1 = 90meV
e1-hh1 (430 meV)
hh1 = 5.5 meV
ΔEv = 50 meV
$InAs_{0.99}N_{0.01}$
(c)

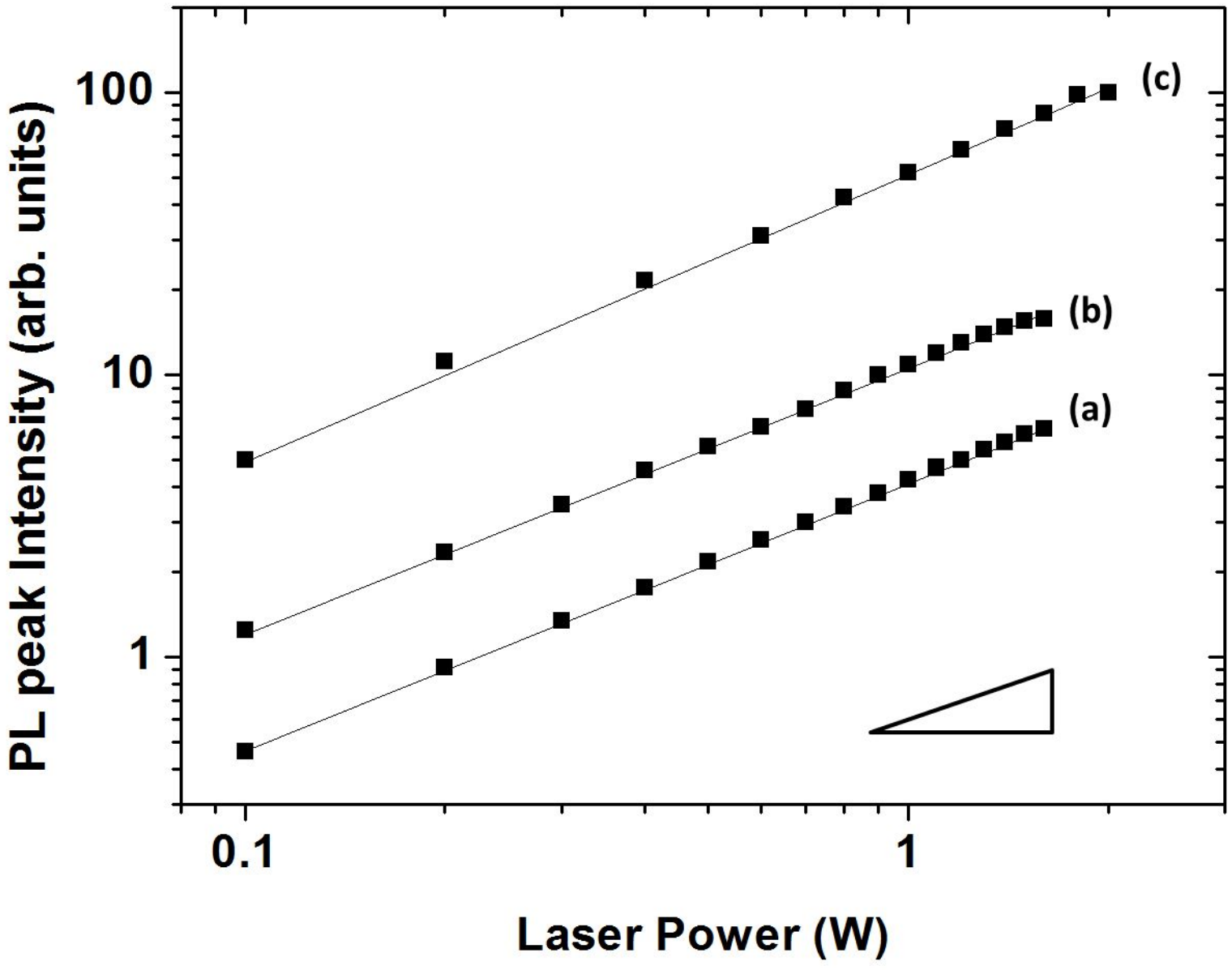
PL peak Intensity (arb. units)
100
10
1
0.1
1
Laser Power (W)
(c)
(b)
(a)

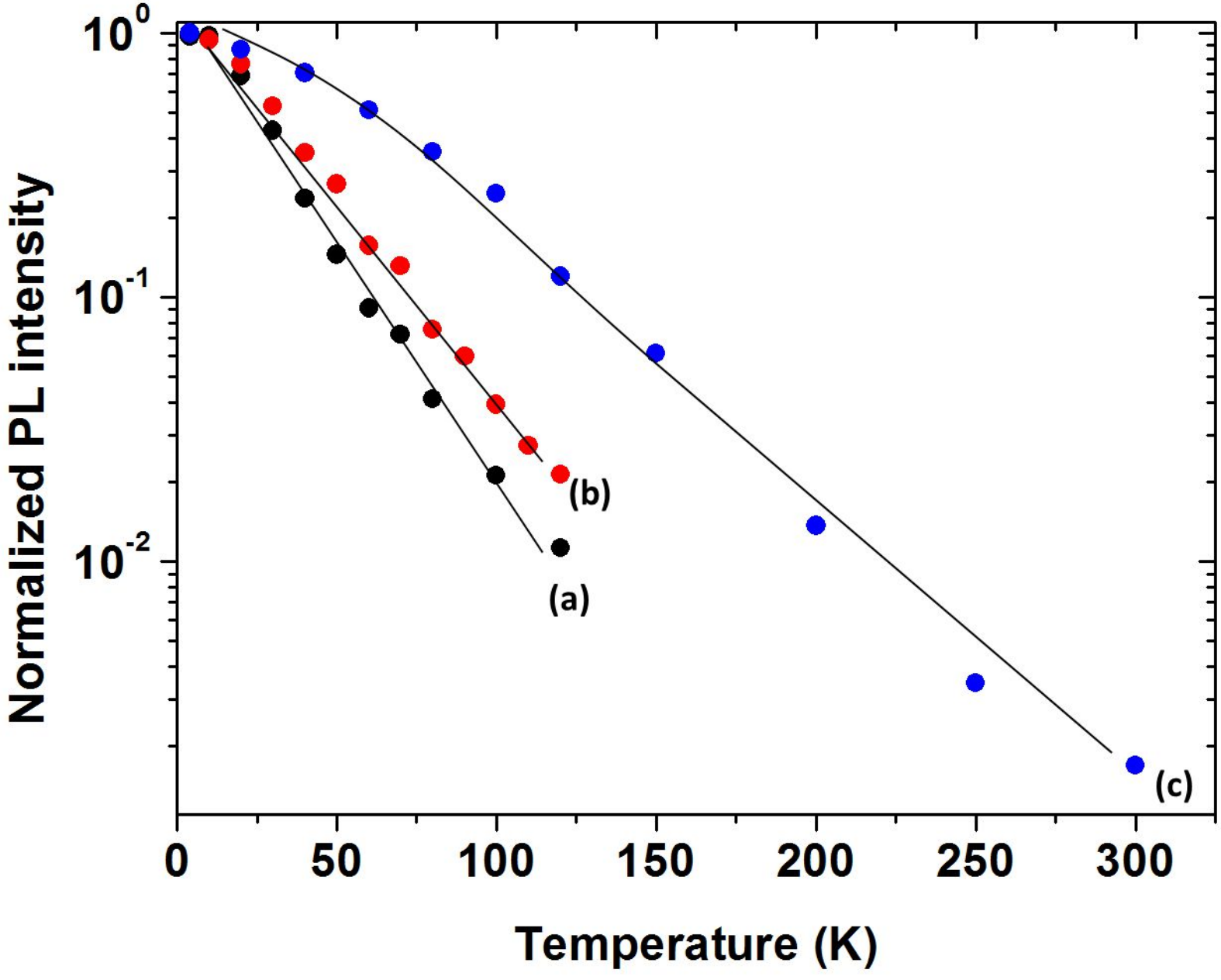
Normalized PL intensity
10^0
10^{-1}
10^{-2}
0
50
100
150
200
250
300
Temperature (K)
(a)
(b)
(c)